Chem. Res. Chinese Universities, 2020, 36(4), 648—661 doi: 10.1007/s40242-020-0171-6

Review

Recent Progress on 2D Transition Metal Compounds-based Electrocatalysts for Efficient Nitrogen Reduction

DONG Wenfei[1#], CHEN Xiaoyu[1#], PENG Juan[1*], LIU Wanyi[1], JIN Xiaoyong[1], NI Gang[1] and LIU Zheng[2,3,4*]

1. State Key Laboratory of High-efficiency Utilization of Coal and Green Chemical Engineering, National Demonstration Center for Experimental Chemistry Education, College of Chemistry and Chemical Engineering, Ningxia University, Yinchuan 750021, P. R. China;

2. School of Materials Science and Engineering, Nanyang Technological University, Singapore 639798, Singapore;

3. CINTRA CNRS/NTU/THALES, Research Techno Plaza, Singapore 639798, Singapore;

4. Environmental Chemistry and Materials Centre, Nanyang Environment and Water Research Institute, Singapore 639798, Singapore

Abstract Ammonia is a commodity chemical with high added value. Electrochemical reduction of nitrogen has great promise for the sustainable synthesis of ammonia in recent years. Because of its rich resources and unique electronic structure and characteristics, 2D transition metal compounds have been used as electrocatalysts for electrochemical reduction of nitrogen for clean and sustainable production of ammonia. This review outlines the latest development in the use of 2D transition metal compounds as high-efficiency electrocatalysts for nitrogen reduction reaction(NRR). First, we introduce the N_2 reduction mechanism, and briefly summarize the performance indicators of the catalyst. Then, we focused on the functionalization of unique 2D materials to design high-performance 2D electrocatalysts in respect of simulation calculation and experimental development. Finally, the current challenges and future opportunities for NRR electrocatalysts are introduced.

Keywords Electrochemical NH_3 synthesis; Transition metal; Nitrogen fixation; Electrocatalysis

1 Introduction

With the progress of society and the development of the global economy, the environmental problems and the energy crisis caused by the increase in the global population are imminent[1,2]. For a long time, ammonia(NH_3) has attracted great attention as a green, economical, and sustainable resource[3,4]. NH_3 is widely used in the production of agricultural fertilizers[5], and as raw materials for the synthesis of organic macromolecular dyes and other polymers[6]. Moreover, NH_3 is a good carbon-free hydrogen storage chemical energy carrier[7]. And it is an indispensable active nitrogen source for explosive production. At present, other fixation methods of nitrogen are also concerned[8,9]. However, the source and synthesis of ammonia have always troubled people. In order to maintain the production of ammonia at the level required to meet the current demand, currently, ammonia production in the world is achieved by the traditional Haber-Bosch process[10]. In this process, always nitrogen(N_2) and hydrogen(H_2) are used as raw materials, and Fe or Ru-based materials as catalysts. It also required a high temperature(500 °C) and high pressure (200—300 atm, 1 atm=1.01×10^5 Pa). The reaction process is shown below[Eq.(1)].

$$N_2 + 3H_2 \longrightarrow 2NH_3 \quad (1)$$

Cunently, the industrial synthesis of ammonia through Haber-Bosch process has great limitations. For example, complex equipment is needed. The reaction also needs high energy consumption, and a large amount of carbon dioxide emissions. It is reported that the industrial production of ammonia consumes much energy from the power supply every year[11]. Thus, it is of great challenge to develop green, sustainable and efficient ammonia synthesis strategies[12].

In recent years, another way to produce ammonia is a low energy nitrogen reduction reaction(NRR)[13]. The reaction formula is as follows:

$$2N_2 + 6H_2O \longrightarrow 4NH_3 + 3O_2 \quad (2)$$

Electrocatalysis is a promising technology that can integrate the electrical energy generated by renewable energy technologies to produce ammonia under ancient conditions. Generally, the electrocatalytic NRR system uses cathode-side nitrogen reduction, as shown in Eq.(3):

*Corresponding authors. Email: z.liu@ntu.edu.sg; pengjuan@nxu.edu.cn

# These authors contributed equally to this work.

Received June 6, 2020; accepted July 7, 2020.

Supported by the Natural Science Foundation of Ningxia, China(No.2018AAC03012), the National Natural Science Foundation of China(No.21765016), the Ningxia Leading Scientific and Technological Innovation Talents Project, China (No.KJT2018002) and the National First-rate Discipline Project of Ningxia, China(NXYLXK2017A04).

$$N_2 + 6H^+ + 6e^- \longrightarrow 2NH_3 \quad (3)$$

Unfortunately, N_2 molecule is very stable and has very high bond energy(about 941 kJ/mol). A highly efficient and durable electrocatalyst must be developed to drive the NRR to achieve NH_3 production[14]. In addition, in the reaction system with water, the electrocatalytic NRR used at the cathode for ammonia synthesis is highly competitive with the electrocatalytic hydrogen evolution reaction(HER). This dramatically reduces the efficiency of nitrogen fixation and the selectivity of the catalyst. Most attempts to synthesize ammonia from N_2 and H_2O are limited by weak catalytic activity and low selectivity of NRR[3].

Two-dimensional(2D) nanomaterials have infinite lateral direction and very small thickness with a regular and ordered grid structure formed by strong in-plane bonding and weak plane simple bonding[15]. Intuitively, 2D nanomaterials can be summarized as allotropes with periodic molecular framework structures or compounds with two or more elements covalently composed[16]. It is expected that the enthusiasm for the research of these 2D nanomaterials is originated from the groundbreaking and Nobel prizes of Novoselov, Geim and colleagues in 2004[17]. They were the first to peel graphene from graphite with tape. At present, 2D nanomaterials have received extensive attention because of their unique physical and chemical properties, which have extended applications in electronics, catalysis, energy storage and power generation, sensing, separation and other related fields[15,17—20]. 2D nanomaterials have aroused great attention in the construction of high-efficiency electrocatalysts due to their adjustable crystal plane size spacing, uniformly exposed lattice plane and unique electronic structure. In addition, the 2D electrocatalysts have the advantages of large specific surface and more exposed catalytic active sites, and it is possible to construct a multi-phase composite catalyst. 2D nanomaterials have proved to be efficient electrocatalysts for electrocatalytic synthesis of ammonia using water and N_2 as reactants. By heteroatom doping and surface engineering, the inherent properties of 2D nanomaterials were changed[4,18,21—23]. These materials have great potential application in the design of high-performance electrocatalysts.

Typical 2D materials include graphene analogs, transition metal(TM) compounds and other layered structure compounds and exhibit excellent electrocatalytic performance for NRR. In particular, TM and their compounds with a layered structure similar to graphene have received extensive attention. Nanomaterials based on 2D TM have been used to electrocatalyze the reduction of nitrogen to produce ammonia[23—25]. The TM compounds are inexpensive, easy to obtain, highly efficient for NRR, and comparable to precious metals. So far, as described in some papers, various TM compounds(including TM carbides and nitrides[22,24], and chalcogenides[23], etc.) have been used as electrocatalysts in NRR system. However, there are few reports on the application and recent development of electrocatalysts based on 2D TMs in NRR for NH_3 production.

This review summarizes a detailed overview of the application of 2D TM compounds and their composite as electrocatalysts in NRR. We summarize important achievements and look forward to the remaining challenges in this hot field. Based on this, we first give a brief introduction of the electrocatalytic NRR reaction mechanism, catalytic activity measurement and analysis. In addition, this review briefly discusses the relationship between 2D TM catalyst and electrocatalytic NRR performance. By summarizing DFT calculations, the importance of composite utilization of 2D TM electrocatalytic nanomaterials in NRR is particularly emphasized. A series of examples covers various 2D TM compounds. In a certain electrocatalysis process, the chemical adsorption energy of the reaction intermediate can be optimized by adjusting the inherent electronic structure of the 2D TM catalyst, so as to achieve a good surface reaction rate. Finally, the development status, existing problems and future development direction of 2D TM compound electrocatalyst are prospected.

2 Mechanism of Electrocatalytic NRR

Generally, there are three accepted reaction mechanisms proposed for electrocatalytic NRR, including the dissociation pathway[Fig.1(A)], the associative pathway[Fig.1(B) and (C)], and the Mars-van Krevelen(MvK) pathway(Fig.2)[26—29]. For the dissociation mechanism, the N≡N bond is broken, and then hydrogenated. An N atom is left on the surface of the catalyst. And these atoms are individually converted into NH_3 molecules. In the Haber-Bosch process for industrial ammonia synthesis, nitrogen reduction follows this mechanism, in which high thermodynamic energy causes the fracture of the N≡N bond. Therefore, the dissociation mechanism is not conducive to NRR under environmental conditions. In contrast, the triple bond in N_2 molecule does not break. In the association

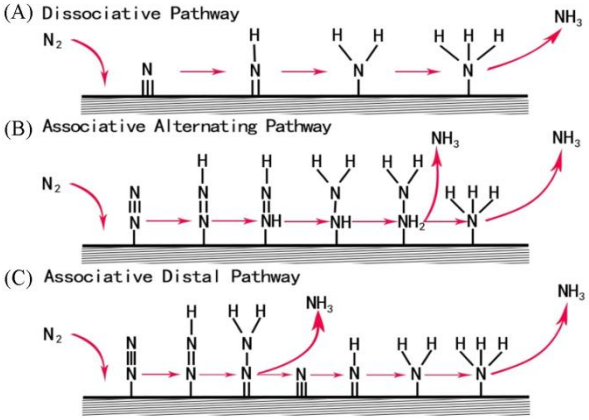

Fig.1 General mechanism of reduction of nitrogen to ammonia[29]

(A) Dissociative pathway, (B) association alternating pathway, (C) associative distal pathway, Copyright 2017, Elsevier Science BV.

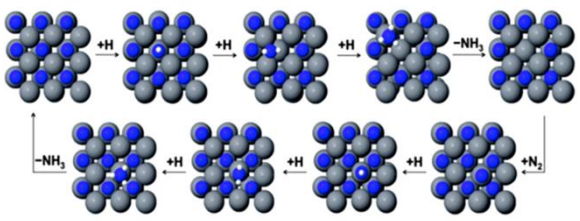

Fig.2 Mvk mechanism for ammonia formation[26]

Copyright 2015, Royal Society Chemistry.

mechanism, two N atoms will combine with each other, while N_2 molecules adsorb on the catalyst surface and undergo hydrogenation. The correlation mechanism may be further divided into distant related pathways and related alternate pathways. In associative alternation, H atoms may react with N atoms, and two NH_3 molecules form a path almost simultaneously. Unlike in associative alternation, in the related remote pathway, hydrogenation may first occur on the N atom to generate NH_3 molecules on the catalyst surface and leave behind the metal≡N, and then hydrogenate it to produce another NH_3. Recently, the MvK mechanism is also presented in Fig.2 to explain the NRR process on the surface of the TM nitrides. Compared with the typical dissociation and association mechanism, this mechanism provides a more favorable reaction mechanism[26]. In the Mvk mechanism, N_2 is reduced on the surface of transition metal nitrides. After completing the first reduction, the catalyst is regenerated by nitrogen, which is different from the traditional association and dissociation mechanism.

Recently, a surface hydrogenation mechanism for N_2 reduction reaction was proposed[30], which can solve the sharp difference between experiments and calculations that have recently appeared. Surface hydrogenation can drive the NRR on catalysts with weak N_2 binding strength(*i.e.*, precious metal catalysts) at low potentials. It was found that the reduction of H^+ instead of N_2 adsorption is the first step, which is also a potential determining step. The total reaction rate is determined by overcoming the relatively high energy barrier. This process can activate N_2 molecule and reduce it to $^*N_2H_2$. Moreover, the synergistic effect of the surface $^*H$ and the catalyst plays an important role in the activation of N_2 molecules.

3 Indicators to Measure Catalyst Performance

The NRR measurement system is divided into an electrochemical reaction part(Fig.3) and a product analysis part. Objectively evaluating the activity of electrocatalysts in NRR systems is an important issue. Therefore, it is necessary to establish a standardized system for catalytic performance measurement. We summarized several key activity indicators that can be used to characterize the catalytic performance of NRR: ammonia yield(a measure of the reaction rate of NH_3 production); Faraday efficiency(FE); and catalyst stability.

3.1 Yield of Ammonia

NH_3 yield refers to the NH_3 production in per unit time and the unit catalyst loading mass(or unit electrode surface area), which reflects the NRR reaction rate of NH_3 synthesis. For electrochemical NRR, the productivity and area/mass of ammonia per unit time are direct parameters to estimate the performance of the catalyst. Table 1 lists the recently reported ammonia production rate of the catalyst. In the experiment, the value can be calculated after the chronoamperometry measurement using the following formula:

$$r(\mathrm{NH_3}) = \frac{n \times v}{t \times m_{\mathrm{cat}}} \tag{4}$$

where $r(NH_3)$ is the formation rate of NH_3 gas, n is the measured NH_3 concentration, V is the volume of the electrolyte, t is the total time of electrolysis, and m_{cat} is the total mass of the catalyst. For membrane catalysts, the area of the electrode(usually the geometric area, and the surface area and electrochemical specific surface area) can be used instead of m_{cat}.

In aqueous solutions and under environmental conditions, the reported $r(NH_3)$ values are mostly in the range of 0.1 to 200 $\mu g \cdot h^{-1} \cdot mg^{-1}cat$. The $r(NH_3)$ values of industrial H-B catalysts are usually in the order of 200—1000 $\mu g \cdot h^{-1} \cdot mg^{-1}cat$[31]. Some representative NRR catalysts reported recently have higher efficiency, such as freestanding 3D graphdiyne-cobalt nitrides[$r(NH_3)$ of 219.72 $\mu g \cdot h^{-1} \cdot mg^{-1}cat$][32].

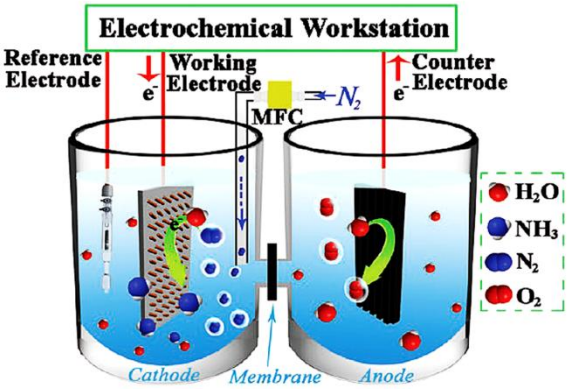

Fig.3 Schematic for electrocatalytic NRR[33]

MFC is the mass flow controller, Copyright 2017, Wiley-VCH.

3.1.1 Spectrophotometric/Colorimetric Methods for the Detection of Ammonia

A potassium tetraiodate($K_2[HgI_4]$) solution called Nessler's reagent is prepared by dissolving a certain amount of anhydrous mercury iodide(HgI_2) and anhydrous potassium iodide(KI) in an alkaline aqueous solution(such as NaOH)[34]. As shown in Eq.(5):

$$\mathrm{NH_4^+ + 2[HgI_4]^{2-} + 4OH^- = HgO \cdot Hg(NH_2)I\downarrow + 7I^- + 3H_2O} \tag{5}$$

Firstly, an appropriate amount of electrolytic solution after electrolytic NRR is drawn from the cathode chamber into the colorimetric tube. A KOH solution is added to adjust the pH of the system. Then, a certain amount of potassium sodium tartrate aqueous solution is added to chelate soluble metal ions. Finally, an appropriate amount of Nessler's reagent is added and diluted to a certain volume with water. After a period of time for color development, the UV-Vis absorption spectrum is measured. A calibration curve is obtained by changing the electrolyte. Before that, in the same way, a series of standard ammonium chloride solutions with known concentrations is used to replace the electrolyte, and a calibration curve is drawn.

3.1.2 Indophenol Blue Colorimetric Method for the Detection of Ammonia

Indophenol blue is usually used for the determination of ammonia in aqueous solutions[35]. First, the appropriate amount of electrolyte in the cathode chamber after NRR electrolysis is drawn into a colorimetric tube. And a NaOH solution

containing salicylic acid and sodium citrate is added. Then, an appropriate amount of NaClO aqueous solution and sodium nitroferricyanide($C_5FeN_6Na_2O$) aqueous solution are added and let the solution stand for a while. The UV-Vis absorption spectrum is measured at an absorbance of 655 nm. The blank solution is used for background correction and measurement solution. Similarly, by changing the electrolyte, a calibration curve is obtained with a series of known concentrations of standard ammonium chloride solution.

The above two methods can effectively detect ammonia in the microenvironment. However, the elimination of experimental interference and the appropriate control of the detection method are particularly important for NRR experimental analysis. During the experiment, the same calibration solution is used as the detection solution. In lower concentration analysis experiments, a known amount of ammonia is added to ensure the accuracy of the detection. It is worth noting that simple and easy-to-use ammonia test strips have recently appeared on the market for quick and simple analysis of experimental results[36,37].

3.1.3 Ion Chromatography for the Detection of Ammonia

The ion chromatography is a type of chromatography that separates ions and polar molecules based on their affinity for ion exchangers[38]. Compared with other analysis methods, ion chromatography is widely recognized. It has the advantages of high sensitivity and good reproducibility. Although this method is complicated and expensive to operate together, it can realize the rapid detection of multiple ions. And various detection systems can be applied by replacing the detector. It is widely used in recent NRR studies to detect the amount of NH_4^+. The conventional detection limit is about 1 μmol/L. The overlap of Na peak and NH_4^+ peak interferes with the detection of ammonium ion(NH_4^+)[39]. In order to eliminate and avoid this problem, switching the column or using a suitable column and eluent is needed, which ensures that trace cations are detected in a general system[40,41].

3.1.4 Isotope Labeling($^{15}N_2$) for the Detection of Ammonia

In the detection of ammonia, ammonia formed by nitrogen sources should receive special attention. If ammonia is produced, the isotope labeling experiment can provide direct evidence of the right source. Considering that in the electrocatalytic process, the electrocatalyst will decompose to produce ammonia. This results in contamination other than NRR for ammonia detection. In general, the feed gas, electrolyte, electrode surfaces, and the decomposition or desorption of the electrocatalysts(especially those containing nitrogen) may themselves lead to contamination of the system. In addition to the conventional Ar control experiment, the quantitative isotope for real-time monitoring experiment also mentions the $^{15}N_2$ experiment to verify the effect of N_2 reduction on ammonia production. When using $^{15}N_2$ as the feed gas, only $^{15}NH_3$ should be generated, excluding other pollution. In ^{1}H NMR spectrum, the triplet and doublet states can clearly distinguish the different chemical shifts produced by ^{14}N and ^{15}N. At this point, the NRR certainty of a given catalyst can be evaluated. However, the high cost of $^{15}N_2$ limits its use in daily experiments.

In recent years, the technology of online detection of ammonia has been well developed, and the combination of flow injection technology and spectrophotometry has been applied. For example, by indophenol blue automatic spectrophotometry combined with capillary flow sampling analysis, a detection limit of 3.6 nmol/L and a linear range of 10—500 nmol/L can be achieved[42]. With the development of the requirements for ammonia detection, there is an urgent need to develop detection methods for reliable detection, more convenient test methods, and real-time monitoring in electrochemical ammonia synthesis experiments. At the same time, the combination of different methods is also developed to get better detection results.

3.2 Faraday Efficiency(FE)

FE refers to the ratio of Faraday current to the total current of a particular product. For electrochemical NRR, FE is an indicator of NRR selectivity compared to competitive HER. The calculation of FE for the reduction of N_2 to NH_3 is shown in the following formula[Eq.(6)]

$$\mathrm{FE}(\mathrm{NH_3}, \%) = \frac{3 \cdot F \cdot c \cdot V}{M(\mathrm{NH_3}) \cdot Q} \times 100\% \tag{6}$$

where F is the Faraday constant(F=96485.3 C/mol), c is the measured concentration, V is the volume of the electrolyte, M is the relative molecular weight and Q is the total charge in units of C.

It is worth noting that in the NRR process, hydrazine(N_2H_4) is a potential product. For the reduction of four-electron nitrogen to hydrazine(N_2H_4), the FE calculation is shown in the following formula[Eq.(7)]:

$$\mathrm{FE}(\mathrm{N_2H_4}, \%) = \frac{4F \cdot c \cdot V}{M(\mathrm{N_2H_4}) \cdot Q} \times 100\% \tag{7}$$

The NRR Faraday total efficiency is the sum of the following two reactions:

$$\mathrm{FE_{NRR}}(\%) = \mathrm{FE}(\mathrm{NH_3})(\%) + \mathrm{FE}(\mathrm{N_2H_4})(\%) \tag{8}$$

3.3 Stability and Reproducibility

In the electrocatalytic processes, the stability of the catalyst is the main problem of NRR. Catalytic stability represents the service life of electrocatalysts used to electrocatalyze NRR. When the catalyst surface is covered with water, oxygen, hydrogen, etc., it will be poisoned, thereby blocking the active site of N_2 adsorption. This affects electrocatalytic NRR that can be continuously cycled, and there are limited reports on stability. Understanding the catalyst deactivation pathways is critical to the design of stable and highly active NRR electrocatalysts. Therefore, it is particularly important to explore and develop *in-situ* or operational characterization techniques.

4 Advanced NRR Electrocatalyst Based on 2D TM Compounds and Composites

2D TM nanomaterials and composite nanomaterials have a

more uniform exposed lattice, and a large number of exposed electrocatalytic active sites[18]. Moreover, 2D TM materials have the characteristics of abundant reserves, strong activity and easy availability, and have made important contributions to the development of electrocatalysts. Initially, catalysts based on 2D TM compounds were constructed and used in HER, OER, ORR, CO_2RR, etc., showing excellent performance. Recently, it has been found that most 2D TM-based materials also exhibit in electrocatalytic NRR excellent performance. Table 1 lists the NRR performance of 2D TM compounds and composites under ambient conditions. It is worth mentioning that some of these electrocatalysts have similar as or even higher performance than precious metal catalysts. This provides a fresh idea for the design and preparation of high-efficiency electrocatalyst for NRR under environmental conditions. The currently studied 2D TM compounds include chalcogenides, oxides, nitrides/carbides, phosphides and their TM single-element 2D materials with excellent NRR performance. These 2D TM compounds exhibit different catalytic mechanisms and design principles. It is easier to identify the active sites of NRR electrocatalyst from theoretical simulation and experimental progress, which thanks to the simple and effective analysis framework structure of 2D transition metal nanomaterials. The development of 2D electrocatalysts is particularly important in electrocatalytic NRR.

Table 1 NRR performance of 2D TM compounds-based electrocatalysts under ambient conditions*

Catalyst	Potential/V(*vs*. RHE)	Electrolyte	NH_3 production rate	FE(%)	Ref.
MoS_2	−0.50	0.1 mol/L Na_2SO_4	8.08×10^{-11} mol·s^{-1}·cm^{-2}	1.17	[43]
AuNPs@MoS_2	–0.30	0.1 mol/L Na_2SO_4 or 0.1 mol/L KOH	25 μg·h^{-1}·mg^{-1}cat (0.1 mol/L KOH)	9.7(0.1 mol/L Na_2SO_4)	[44]
Ru/2H-MoS_2	−0.15	0.01 mol/L HCl	1.14×10^{-10} mol·cm^{-2}·s^{-1} at 50 °C	17.6	[45]
F doped MoS_2	–0.20	0.05 mol/L H_2SO_4	35.7 μg·h^{-1}·mg^{-1}cat	20.6	[46]
Co-doped MoS_{2-x}	–0.3(*vs*. Ag/AgCl)	0.01 mol/L H_2SO_4	0.63×10^{-3} mol·h^{-1}·g^{-1}cat	10	[47]
MoS_2-rGO	–0.45	0.1 mol/L $LiClO_4$	24.82 μg·h^{-1}·mg^{-1}cat	4.58	[48]
Fe_3S_4 NSs	−0.40	0.1 mol/L HCl	75.4 μg·h^{-1}·mg^{-1}cat	6.45	[49]
FeS_2-Mo_x[a] NSs	−0.20	0.1 mol/L KOH	26.15 μg·h^{-1}·mg^{-1}cat	14.41	[50]
Sn/SnS_2	−0.80	0.1 mol/L PBS	23.8 μg·h^{-1}·mg^{-1}cat	6.5(−0.7 V *vs*. RHE)	[51]
Fe-ReS_2@N-CNF	−0.20	0.1 mol/L Na_2SO_4	80.4 μg·h^{-1}·mg^{-1}cat	12.3	[52]
TiS_2 NSs	−0.60	0.1 mol/L Na_2SO_4	16.02 μg·h^{-1}·mg^{-1}cat	5.50	[53]
Mo-doped SnS_2 NSs	–0.50	0.5 mol/L $LiClO_4$	41.3 μg·h^{-1}·mg^{-1}cat	20.8(–0.4 V *vs*. RHE)	[54]
$NbSe_2$	–0.45	0.1 mol/L Na_2SO_4	89.5 ± 6.0 μg·h^{-1}·mg^{-1}cat	13.9±1.0(–0.40 V *vs*. RHE)	[55]
TiO_2 NSs	−0.80	0.1 mol/L H_2SO_4	35.6 μg·h^{-1}·mg^{-1}cat	5.3(−0.7 V *vs*. RHE)	[56]
TiO_2 NSs	−0.70	0.1 mol/L Na_2SO_4	9.16×10^{-11} mol·s^{-1}·cm^{-2}	2.50	[57]
Y_2O_3 NSs	−0.90	0.1 mol/L Na_2SO_4	1.06×10^{-10} mol·s^{-1}·cm^{-2}	2.53	[58]
MoO_3 NSs	−0.50	0.1 mol/L HCl	4.80×10^{-10} mol·s^{-1}·cm^{-2} (29.43 μg·h^{-1}·mg^{-1}cat)	1.9(−0.3 V *vs*. RHE)	[59]
R-WO_3 NSs	−0.30	0.1 mol/L HCl	17.28 μg·h^{-1}·mg^{-1}·mg^{-1}cat	7.0	[60]
Au/TiO_2	−0.40	0.01 mol/L HCl	64.6 μg·h^{-1}·mg^{-1}cat	29.5	[61]
Ru/TiO_2-Vo	−0.15	0.1 mol/L KOH	2.11 μg·h^{-1}·cm^{-2}	0.72	[62]
Au/CoO_x	–0.50	0.05 mol/L H_2SO_4	15.1 μg·h^{-1}·cm^{-2}	19	[63]
C@CoS@TiO_2	–0.55	0.1 mol/L Na_2SO_4	8.09×10^{-10} mol·s^{-1}·cm^{-2}	28.6	[64]
N-C@NiO/GP	–0.20	0.1 mol/L HCl	14.022 μg·h^{-1}·mg^{-1}cat (1.15×10^{-10} mol·s^{-1}·cm^{-2})	30.43	[65]
N-NiO/CC	−0.50	0.1 mol/L $LiClO_4$	22.7 μg·h^{-1}·mg^{-1}cat	7.3	[66]
F-SnO_2 NSs	−0.45	0.1 mol/L Na_2SO_4	19.3 μg·h^{-1}·mg^{-1}cat	8.6	[67]
$Ti_3C_2T_x$ NSs	−0.20	0.5 mol/L Li_2SO_4(pH=2)	0.53 μg·h^{-1}·cm^{-2}	5.78	[68]
$Ti_3C_2T_x$ NSs	−0.40	0.1 mol/L HCl	20.4 μg·h^{-1}·mg^{-1}cat	9.3	[69]
$Ti_3C_2T_x$(T=O, OH) NSs	−0.30	0.1 mol/L HCl	36.9 μg·h^{-1}·mg^{-1}cat	9.1	[70]
Ru@Ti_3C_2 MXene	−0.40	0.1 mol/L KOH	2.3×10^{-6} mol·h^{-1}·cm^{-2}	13.13	[71]
TiO_2/$Ti_3C_2T_x$	−0.60	0.1 mol/L HCl	26.32 μg·h^{-1}·mg^{-1}cat	8.42	[72]
TiO_2/$Ti_3C_2T_x$	−0.45	0.1 mol/L HCl	32.17 μg·h^{-1}·mg^{-1}cat(−0.55 V *vs*. RHE)	16.07	[73]
MnO_2-$Ti_3C_2T_x$	–0.55	0.1 mol/L HCl	34.12 μg·h^{-1}·mg^{-1}cat	11.39	[74]
MoN NSs	−0.30	0.1 mol/L HCl	3.01×10^{-10} mol·s^{-1}·cm^{-2}	1.15	[75]
VN NSs array	−0.50	0.1 mol/L HCl	8.4×10^{-11} mol·s^{-1}·cm^{-2}	2.25	[76]
W_2N_3 NSs	−0.20	0.1 mol/L KOH	(11.66±0.98) μg·h^{-1}·mg^{-1}cat	11.67±0.93	[77]
LaF_3 NPs	–0.45	0.5 mol/L $LiClO_4$	55.9 μg·h^{-1}·mg^{-1}cat	16.0	[78]
$La_2Ti_2O_7$ NSs	−0.55	0.1 mol/L HCl	25.15 μg·h^{-1}·mg^{-1}cat	4.55	[79]
$K_2Ti_4O_9$	–0.50	0.1 mol/L KOH	22.88 μg·h^{-1}·mg^{-1}cat	5.87	[80]

* CC: carbon cloth; rGO: reduced graphene oxide; NPs: nanoparticles; NSs: nanosheets; d-TiO_2/TM: defective TiO_2 on Ti mesh; Vo: oxygen-vacancy; GP: graphite paper; T: F, OH; x[a]: the atomic percentage of Mo atoms in all metallic ions.

4.1 TM Chalcogenides

So far, many 2D TM-based electrocatalysts of NRR have been developed. Among them, TM chalcogenides, such as MoS_2, MoSSe, SnS_2, ReS_2, TiS_2, InSe, GaSe, $NbSe_2$ and the composite materials have been constructed with excellent

catalytic activity and low cost[43—49,51—53,55,81]. Many promising properties of TM chalcogenides have been explored. Vacancy engineering and heteroatom doping are two effective methods to adjust the electronic structure of the catalyst to improve the electrocatalytic activity[47,52,54,82,83]. In addition, a lot of researches have also been done on the combination of TM chalcogenide compounds with other materials to further improve catalytic efficiency and stability. In electrocatalytic NRR, the hybridization of TM chalcogenide compounds with other nanomaterials(such as precious metals and conductive materials) can provide more active sites, ensuring rapid electron transfer between external circuits and electrodes, thereby improving electrocatalysis NRR activity[44,48]. More importantly, excellent design and manufacture of TM chalcogenide-based composite catalysts requires an in-depth understanding of important basic mechanisms of NRR electrocatalysis, such as synergistic effects, heterostructures, defects and strain impact[47,84]. 2D TM chalcogenide-based composites can be considered as an efficient strategy to build low-cost, high-efficiency NRR catalysts for their future applications. Here, we will focus on the development of catalytic composites based on 2D TM chalcogenide compounds in recent years.

4.1.1 Theoretical Simulation(S, Se)

The development of low-cost, high-efficiency materials for electrocatalytic nitrogen reduction is an attractive and challenging topic in the field of electrocatalysis. 2D electrocatalyst supported single-atom catalyst(SAC), due to 100% utilization of atoms, high activity and high selectivity, has recently been widely used in electrochemical NRR[85—87]. To this end, many theoretical studies have been published to demonstrate the potential of 2D TM chalcogenide catalysts and composite nanomaterials for NRR electrocatalytic synthesis of ammonia[83—89].

Recently, Ge's group[85] used density functional theory (DFT) calculations to systematically study the electrocatalytic performance of a series of TM atoms loaded on MoS_2 nanosheets(TM@MoS_2). The study found that Re loaded on MoS_2(Re@MoS_2) has the best NRR catalytic activity whith a limit potential being –0.43 V, and has a high selectivity for the competitive HER. Feng's group[86] reported that the single atom of the TM was anchored on a single layer of MoS_2 as a potential substrate. The electro-catalytic NRR of MoS_2(Mo@MoS_2-M) screened by the first principle high-throughput is a process with a higher selectivity for NRR through the remote mechanism than that of HER. The estimated overpotential of Mo@MoS_2-M is about 0.28 V for NRR. Chen's group[87] used DFT calculations to explore the feasibility of defective MoS_2 sheets as a matrix to embed a series of single TM atoms as an NRR electrocatalyst. The free energy distribution diagram from the reaction(Fig.4) shows that the insertion of single TM atoms is easier to break the N≡N bond and promote the activation of N_2. Yang *et al.*[88] calculated the 1T-MoS_2 decorated with V through DFT and showed excellent catalytic activity for NRR through a remote mechanism. The corresponding initial potential is 0.66 eV, which is superior to those of the commercial Ru materials. In addition, the strong binding energy between V atoms and 1T-MoS_2 provides good resistance to the aggregation of V dopants, indicating its stability.

Tang's group[82] compared the electrocatalytic performance of single-atom and diatomic modified MoS_2 through DFT calculation. The single layer of MoS_2 doped with boron atoms(B_2@MoS_2) was used as a potential electrocatalyst for NRR. The theoretical simulation found that the catalyst modified by double atoms showed more excellent structure and thermodynamic stability. At the same time, it was found that the diatomic modification showed a significant increase in the electrical conductivity of MoS_2. The author also found that the overpotential for electrocatalytic NRR(B_2@MoS_2) is much lower than that of other reported single-atom catalysts, and its excellent activity benefits from the synergistic effect of effective electron transport and diatoms.

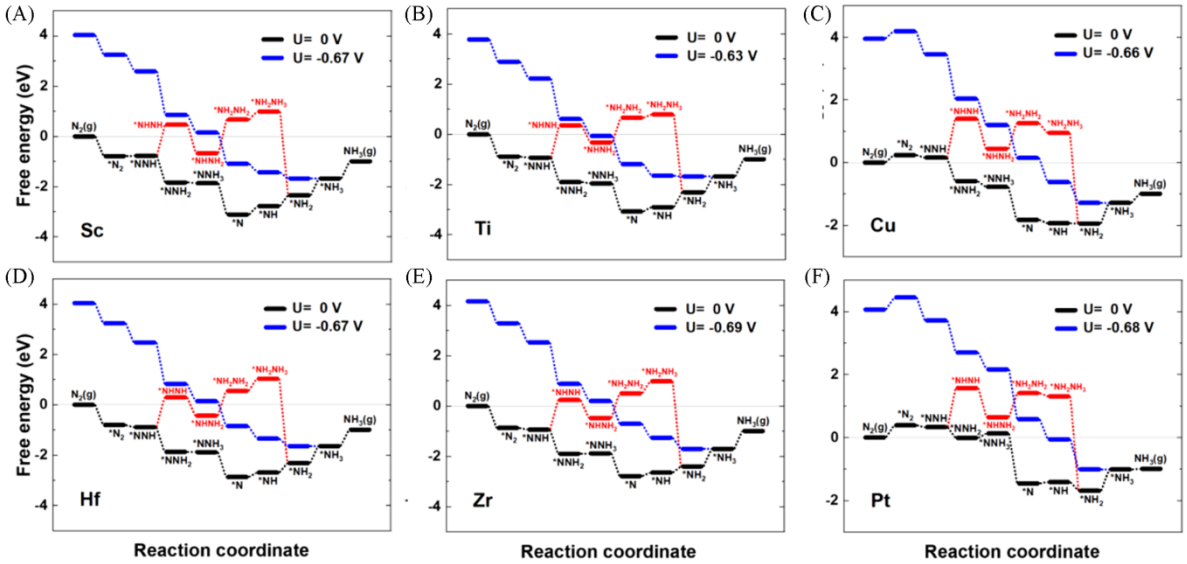

Fig.4 Free energy spectrum of reaction pathway[87]

The red line indicates the alternate mechanism; the blue line indicates the distal mechanism, and the black line indicates no potential. The asterisk(*) indicates the adsorption site. Copyright 2019, American Chemical Society.

Ma *et al.*[83] showed that boron-doped InSe(B-InSe) has excellent electrocatalytic activity by DFT calculation. B-InSe strongly attracts N_2 and H near the catalytic center of B, and has unstable adsorption at other surface sites, so it can well avoid competitive HER. With the adsorption of N_2, B ions exchange electrons with N_2 through the acceptor mode. The B-InSe monolayer provides new opportunities for NRR's highly efficient electrocatalyst. Huang's group[84] reported how to use the size of defects to adjust NRR performance. It is predicted that the Ga atoms exposed in the 2D defect gallium selenide monolayer(V-GaSe) can exhibit excellent NRR electrocatalytic performance. As shown in the Fig.5(A) and (B), due to the pulling effect, Ga atoms can capture N_2 molecules. In this process, the conversion of N_2 to NH_3 becomes easier due to the increased adsorption capacity of nitrogen. The potential is 0.3 V on V-GaSe strained at 8% as shown in Fig.5(C). At the same time, the author further designed the Janus V-GaInSe$_2$ structure. On the 4% strained V-GaInSe$_2$, the simulated starting point was –0.31 V, which is equivalent to 8% strained V-GaSe. The authors show that as the strain changes, the hydrogen evolution reaction can be suppressed. Li's group[89] reported that based on DFT, the performance of a series of S or Se-containing TMs embedded in MoSSe nanosheets as a potential electrocatalytic NRR was calculated. The results show that the nanosheets with vacancies show better catalytic performance when embedded in Mo, which is proved by the high stability of the adsorbed N_2H species. MoSSe embedded in Mo has huge catalytic activity. The Mo-doped MoSSe has higher selectivity in ammonia synthesis reaction.

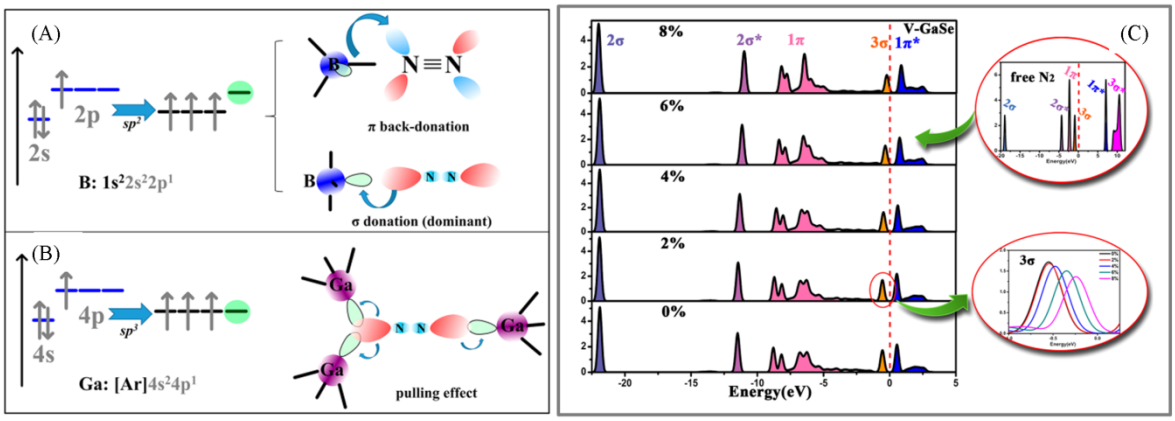

Fig.5 Hybridization diagram and catalyst DOS diagram[84]

(A) B element and catalytic principle; (B) Ga element; (C) DOS of V-GaSe. The upper inset is the DOS of the free N_2 molecule; the lower inset shows the trend in the 3σ orbital with respect to the strain. Copyright 2020, American Chemical Society.

4.1.2 Experimental Progress

2D TM chalcogenide compounds have attracted much attention in electrocatalytic NRR reactions due to their high surface area, optimized N_2 absorption energy, and adjustable electronic structure. 2D TM chalcogenide compounds[43,55] and supported precious metal nanocatalysts[44,45], non-metallic element doping[46], other TM element doping[47,50—52,54] were designed to build NRR catalysts[48].

Sun's research group[43] used MoS_2 nanosheet electrochemical tests to show that the catalyst in 0.1 mol/L Na_2SO_4 can achieve high FE(1.17%) and high NH_3 yield(8.08×10^{-11} mol·s^{-1}·cm^{-1}cat) at –0.5 V(*vs.* RHE). MacFarlane's group[45] reported Ru/MoS_2 electrocatalysis has high selectivity and theoretically proved that high-performance electrocatalysts benefit from the cooperative interaction between Ru cluster sulfur vacancies. At 50 °C, the FE is as high as 17.6%, and the NH_3 yield is 1.14×10^{-10} mol·cm^{-2}·s^{-1}. Zhang's group[44] has grown AuNPs on MoS_2 tablets, and the AuNPs@MoS_2 prepared showed excellent electrocatalytic activity under all pH conditions. The best NRR electrode potential is –0.3 V, relative to RHE. Among them, the NRR in 0.1 mol/L Na_2SO_4 showed the highest FE of 9.7%, and the highest average NH_3 yield(25 μg·h^{-1}·mg^{-1}cat) in 0.1 mol/L KOH. The ultra-stable crystal structure of AuNPs@MoS_2 has strong dispersibility. Liang *et al.*[46] have reported the use of strain engineering strategies to incorporate F ions into defect-rich MoS_2 nanosheets to compress the interlayer space of MoS_2. The experimental results prove that under acidic conditions, the activity and selectivity of the electrochemical NRR of F-doped MoS_2(F-MoS_2) catalyst are significantly improved. The FE of F-MoS_2 for electrocatalytic NRR increased to 20.6%. At –0.2 V(*vs.* RHE), the NH_3 yield was as high as 35.7 μg·h^{-1}·mg^{-1}cat. Lou's group[47] studied the modification of the MoS_{2-x}-based surface by Co doping to act as a catalyst to mimic the sulfur vacancies in the active site of natural Mo-nitrogenase. The electrocatalyst showed excellent NRR activity. The DFT simulation results show that the free energy barrier after Co doping is reduced from 1.62 eV to 0.59 eV, and the free energy barrier can be compensated by applying an overpotential. At the same time, defective MoS_{2-x} can adsorb N_2, making the catalyst decompose N≡N triple bond more effectively. Due to the modulation of the Mo—N bond structure, Co doping further accelerates this process. Li *et al.*[48] reported that MoS_2 nanosheets on reduced graphene oxide hybrid(MoS_2-rGO) can be used as a high-performance NRR catalyst. In 0.1 mol/L $LiClO_4$, the FE of the catalyst is as high as 4.58%, and the NH_3 yield is as high as 24.82 μg·h^{-1}·mg^{-1}cat at –0.45 V(*vs.* RHE).

Jia *et al.*[53] reported that TiS_2 nanosheets(TiS_2 NSs) are highly efficient NRR electrocatalysts. The TiS_2 NSs can achieve a high FE of 5.50% at –0.60 V(*vs.* RHE) and a large

NH_3 yield 16.02 μg·h^{-1}·mg^{-1}cat in 0.1 mol/L Na_2SO_4. Wang *et al.*[81] reported NbS_2 nanosheets obtained by mechanical exfoliation. Due to more exposed active sites and high electron transfer capabilities, the exfoliated NbS_2 nanosheets have extraordinary activity for electrochemical NRR. A high FE of 10.12% and an NH_3 yield of 37.58 μg·h^{-1}·mg^{-1}cat can be achieved at –0.50 V(*vs*. RHE). The Nb^{4+} species of exfoliated NbS_2 was confirmed as the active site of NRR. Luo's group[55] has prepared a self-supporting $NbSe_2$ nanosheet array($NbSe_2$ NSA), as shown in Fig.6(A)—(E). At –0.4 V(*vs*. RHE), the FE is 13.9%±1.0%. At –0.45 V(*vs*. RHE), the yield of NH_3 in 0.1 mol/L Na_2SO_4 is (89.5±6.0) μg·h^{-1}·mg^{-1}cat. In addition, during the 60-h electrolysis, the efficiency of the electrocatalyst and the NH_3 yield did not decrease steadily[Fig.6(F)—(I)]. In addition, DFT calculations show that $NbSe_2$ can effectively catalyze the dissociation of adsorbed N_2 molecules, thereby promoting the NRR process. Zhao *et al.*[49] reported the Fe_3S_4 nanosheets as a new NRR electrocatalyst. The obtained Fe_3S_4 nanosheets have a higher NH_3 yield(75.4 μg·h^{-1}·mg^{-1}cat) and an FE(6.45%) at –0.4 V(*vs*. RHE).

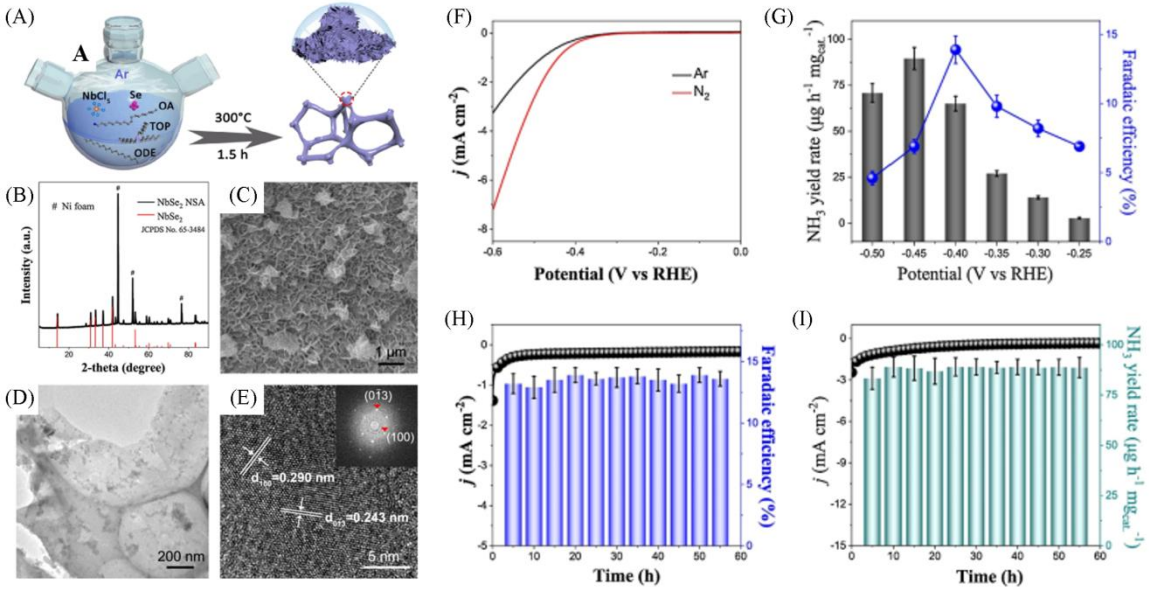

Fig.6 Synthesis and characterization of $NbSe_2$ NSA, NRR performances under ancient conditions[55]

(A) Schematic illustration of the synthetic procedure; (B) XRD pattern; (C) SEM image; (D) TEM image; (E) HRTEM image. The inset in (E) is the corresponding FFT pattern; (F) LSV curves in Ar- and N_2-saturated 0.1 mol/L Na_2SO_4 solution; (G) calculated FEs and yield rates of NH_3 at different potentials; (H) FEs at −0.40 V *vs*. RHE during the 60-h electrolysis; (I) NH_3 yield rates at −0.45 V *vs*. RHE during the 60-h electrolysis. The error bars correspond to the standard deviations of six measurements. Copyright 2020, Elsevier.

Inspired by natural nitrogenase, Wang *et al.*[50] designed a inorganic catalyst, FeS_2 doped with Mo(IV), to NRR. The FeS_2-Mo catalyst shows obvious advantages in N_2 adsorption and activation, so the FE is as high as 14.41% at –0.2 V(*vs*. RHE). Li *et al.*[51] synthesized various amorphous Sn/crystalline SnS_2(Sn/SnS_2) nanosheets. At –0.8 V(*vs*. RHE) in 0.1 mol/L PBS, the fixed Sn/crystalline SnS_2 electrocatalyst can achieve a high NH_3 yield of 23.8 μg·h^{-1}·mg^{-1}cat and a high FE of 6.5% at –0.7 V(*vs*. RHE). Chen's group[52] reported that low-valent TMs doped in ReS_2 provide more active sites for NRR electrocatalytic electron transfer, weakening N—N/O—H. It was found that the FeS-doped ReS_2 nanosheets wrapped with N-doped C nanofibers catalyst had excellent electrochemical activity. The ammonia yield was 8 times higher, at 80.4 μg·h^{-1}·mg^{-1}cat. The Tafel slope is 63 mV/dec. The Mo-doped SnS_2 nanosheets with enriched sulfur vacancies(V_s) developed by Guo's group[54] exhibited significantly enhanced NRR activity, with an NH_3 yield of 41.3 μg·h^{-1}·mg^{-1}cat(–0.5 V *vs*. RHE) and an FE of 20.8%(–0.4 V *vs*. RHE). Mechanism research shows that the co-existence of Mo dopant and V_s can form the catalytic site of Mo-Sn-Sn trimer, even if the N≡N triple bond is broken into N=N under N_2 adsorption. The N double bond can also strongly activate the N_2 phase, thus greatly reducing the energy barrier of the first hydrogenation step.

4.2 TM Oxides

It is particularly important to produce 2D electrocatalysts with high NRR activity and selectivity through rationally designed structural engineering. 2D TM oxide is expected to be a hopeful catalyst for NRR due to its good electrical conductivity. However, the inherent activity of these materials is poor, which hinders their further development. Taking advantage of the advantages of 2D nanomaterials itself to develop NRR electrocatalysts has great advantages. The doping of precious metal nanoparticles and other elements to control the electronic structure of 2D TM oxides can induce enhanced surface conductivity and d-band centers, thereby constructing vacancies and defects to further expand the reactive center of nanomaterial electrocatalyst NRR. At the same time, it is compounded with other sheet-like nanomaterials to prevent the nanomaterials from agglomerating to form heterojunctions, thereby generating rapid reaction kinetics in constructing the heterogeneous interface. The specific experimental applications are discussed below.

Sun's group[57] modified TiO_2 nanosheets on a titanium plate(TiO_2/Ti) to form an array of electrocatalytic NRR with excellent selectivity and high electrochemical stability. The excellent NRR activity is due to the *in-situ* generation of

oxygen vacancies during electrochemical testing that enhances the adsorption and activation of N_2. In 0.1 mol/L Na_2SO_4 at –0.7 V *vs*. RHE, TiO_2/Ti has a high NH_3 yield of 9.16×10^{-11} $mol\cdot s^{-1}\cdot cm^{-2}$, corresponding to an FE of 2.50%. The oxygen-containing vacancy TiO_2 nanosheets with high-selectivity and high-stability have been reported by Fang *et al*.[56]. The TiO_2 nanostructures were prepared by annealing at different temperatures in an H_2/Ar atmosphere to introduce and adjust oxygen vacancies, as shown in Fig.7. DFT calculations prove that oxygen vacancy can greatly reduce the energy barrier to activate the inert N≡N bond for N_2 fixation. The TiO_2 nanosheets provide abundant active centers on its surface to improve the reaction on its surface. The highest NH_3 yield is as high as 35.6 $\mu g\cdot h^{-1}\cdot mg^{-1}$cat, and the FE is 5.3%. Sun's group[59] reported that MoO_3 nanosheets as an efficient and very selective NRR electrocatalyst. In 0.1 mol/L HCl, the NH_3 yield was 4.80×10^{-10} $mol\cdot s^{-1}\cdot cm^{-2}\cdot mg^{-1}$(29.43 $\mu g\cdot h^{-1}\cdot mg^{-1}$cat). And the FE was 1.9%. DFT calculations show that the outermost Mo atoms act as active sites for the effective adsorption of N_2. Li's group[58] proved that Y_2O_3 nanosheets have excellent stability and durability and can be used as an efficient NRR electrocatalyst. The Y_2O_3 nanosheet has a large NH_3 yield of 1.06×10^{-10} $mol\cdot s^{-1}\cdot cm^{-2}$ and an FE of 2.53% at −0.9 V *vs*. RHE. Kong *et al*.[60] demonstrated that WO_3 nanosheets rich in oxygen vacancies(R-WO_3 NSs) exhibited great NRR performance. This R-WO_3 NS can achieve a large NH_3 yield of 17.28 $\mu g\cdot h^{-1}\cdot mg^{-1}$cat and a high FE of 7.0% at –0.3 V *vs*. RHE.

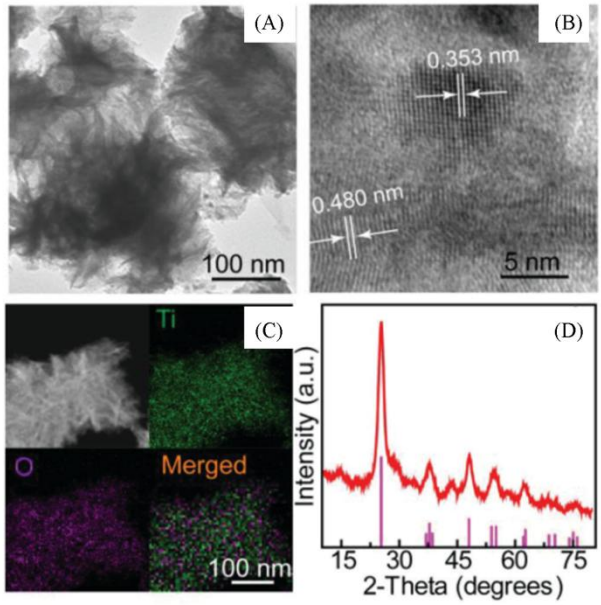

Fig.7 Structure characterization of OV-TiO_2-400[56]

(A) TEM image; (B) HRTEM image; (C) EDX elemental mappings; (D) XRD patterns of the OV-TiO_2-400, Copyright 2019, Wiley-VCH.

Guo's group[61] introduced 2D gold(Au/TiO_2) enriched in oxygen vacancies, which can be used as an advanced NRR electrocatalyst. As shown in Fig.8, the morphology, structure and composition of 2%(mass ratio) Au/TiO_2 nanosheets were prepared. The electrocatalytic test shows that the Au/TiO_2 hybrid catalyst has an NH_3 yield of 64.6 $\mu g\cdot h^{-1}\cdot mg^{-1}$cat and an FE of 29.5% at –0.40 V *vs*. RHE. Experimental results and theoretical calculations show that oxygen vacancies in TiO_2 have a strong electron-donating effect, which is crucial for the activation of N_2. The introduction of Au promotes electrochemistry and thermodynamics by adjusting the electronic structure of the active site speed limit steps. Wang's group[62] reported that the TiO_2-O vacancies obtained after calcination at a high temperature had thicker and smaller 2D nanosheets. The final Ru/TiO_2-O vacancies were obtained by heat treatment of $Ru(acac)_3$ and loading with Ru NPs. The electrocatalysis results show that Ru/TiO_2-Vo shows good NRR performance(2.11 $\mu g\cdot h^{-1}\cdot cm^{-2}$). In addition, the DFT calculation results show that the NRR catalytic mechanism and rate determination step ($^*N_2 + 1/2H_2 \longrightarrow {}^*N + {}^*NH$) is the potential determination step, and the overpotential requirement is 0.21 V. Electronic structure analysis and catalytic measurements reveal the synergistic effect of ruthenium and oxygen vacancy on NRR performance. Wang's group[63] reported on changing the oxidation state of Au to control NRR in the production of valuable NH_3. Au nanoparticles were introduced with positive valence into the CoO_x layer(Au/CoO_x) to regulate the local electronic structure, and thus promote the conversion of N_2 to NH_3. At –0.5 V(*vs*. RHE), the Au/CoO_x catalyst has a higher average oxidation state(about 40%), achieving a high NH_3 yield of 15.1 $\mu g\cdot cm^{-2}\cdot h^{-1}$ and an FE of 19%. Experimental and simulation results show that the ability to adjust the oxidation state of Au can control the N_2 energy barrier of NRR.

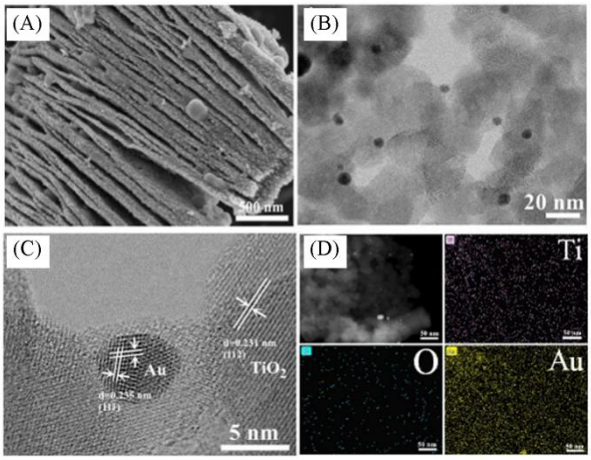

Fig.8 Structure characterization of Au/TiO_2[61]

(A) SEM image; (B) TEM image; (C) HRTEM image; (D) EDS mapping images of $AuTiO_2$, Copyright 2020, Royal Society Chemistry.

Liu *et al*.[67] reported that F-doped SnO_2 mesoporous nanosheets on carbon cloth(F-SnO_2/CC) were used as effective NRR electrocatalysts. The F-SnO_2/CC showed high NRR activity, NH_3 yield was 19.3 $\mu g\cdot h^{-1}\cdot mg^{-1}$cat. The FE was 8.6% at –0.45 V(*vs*. RHE) in 0.1 mol/L Na_2SO_4. The excellent performance is attributed to the combination of sheet structure and F-doping has structural advantages. DFT calculations show that F-doping can easily adjust the electronic structure of SnO_2 to make it more conductive, and increase the positive charge at the active Sn position, thereby reducing the reaction energy barrier and increasing NRR activity. The application of heterogeneous interface engineering has a very good role in

improving electrocatalytic kinetics. Based on this, Liu *et al.*[64] anchored CoS nanosheets on TiO_2 nanofiber membranes, and further improved the material's conductivity through carbon nanoplating. The obtained NRR electrocatalyst C@CoS@TiO_2 has a high NH_3 yield(8.09×10^{-10} mol·s^{-1}·cm^{-2}) and a hight FE(28.6%). This interface design significantly improves NRR performance, as well as excellent long-term durability.

Komarneni's group[65] reported a kind of N-doped porous carbon distributed on graphite paper spontaneously grown on nickel oxide nanosheets(NC@NiO/GP). The NH_3 yield at –0.2 V(*vs*. RHE) reached 14.022 μg·h^{-1}·mg^{-1}cat(1.15×10^{-10} mol·s^{-1}·cm^{-2}). Its FE exceeds 30.43%. The composite material also has excellent electrocatalytic activity and electrocatalytic time up to 20 h. Chu's group[66] reported that nitrogen-doped NiO nanosheet arrays(N-NiO/CC) on carbon cloth were used as NRR model heteroatom-doped TM-based electrocatalysts. The NH_3 yield in 0.1 mol/L $LiClO_4$ at –0.5 V(*vs*. RHE) for N-NiO/CC is 22.7 μg·h^{-1}·mg^{-1}cat, and the FE value is 7.3%. DFT calculations show that N-doping can induce enhanced surface conductivity and d-band center, thereby improving the stability of *NNH, lowering the reaction energy barrier, and thus improving NRR performance.

4.3 TM Nitrides/Carbides

In recent years, 2D TM nitrides/carbides have a large specific surface area due to their unique layered structure, and have significant advantages in the field of energy storage and catalysis[22,24]. The 2D TM carbide, carbonitride and nitride (collectively MXenes) families are novel 2D nanomaterials. Since Ti_3C_2 was discovered in 2011[90], it has been widely reported[68—74,91—94]. MXene is a very promising substrate. In the field of photocatalysis[95] and electrocatalysis[96], it has attracted great attention. TM nitrides, such as MoN[75] , W_2N_3[77] and VN[76] nanosheets and their composite nanomaterials have become important electrocatalysts for NRR. Here, we summarize the application of MXene materials in electrocatalytic NRR.

4.3.1 Theoretical Simulation

Understanding the reactivity and stability of different crystal structures and crystal planes of different nanomaterials helps to obtain high-performance NRR polycrystalline materials. For 2D TM nitrides/carbides materials, although the theoretical input energy required for the NRR electrocatalyst process may be underestimated, this method can strongly prove that the trend of 2D MXenes materials in the electrocatalytic synthesis of ammonia is correct, and it is also valuable. Therefore, DFT theoretical simulation can well predict the performance of the material, and it can be combined with experiments well to prove the mechanism.

Abghoui *et al.*[97—101] designed and studied the electrocatalytic nitrogen fixation performance of different structure nitrides of rock salt(RS) and zincblende(ZB) based on DFT theory. Theoretical results prove that VN, CrN, NbN and ZrN of RS(100) structure with lower initial potentials are the most likely candidates. Later, they screened a series of transition metal nitrides with RS(111) or ZB(110) planes[100]. As far as the RS(111) plane is concerned, CrN, VN, MoN, WN, and NbN have been selected to have lower initial potentials, and are good candidates for electrocatalysts for NRR. Recently, Li and colleagues reported[25] that under environmental conditions, Fe-doped MoN_2 nanoflakes greatly reduce the energy required for surface reactions, combined with pure MoN_2 nanoflakes, which have excellent adsorption and activation properties of N_2. The required overpotential is –0.47 V. Azofra *et al.*[96] used DFT to make the assumption that MXene is a promising material for capturing N_2. N_2 chemically adsorbed on MXene undergoes elongation/weakening of the N≡N triple bond, thus it promotes its ability to catalyze the conversion to NH_3 under mild conditions. Specifically, N_2 activation can be achieved spontaneously when N_2 is chemically adsorbed on MXene nanosheets. It is theoretically proved that the V_3C_2 and Nb_3C_2 materials exhibit a strong catalytic conversion performance to NH_3, and the maximum overpotentials are 0.64 and 0.90 V, respectively(*vs*. SHE). Shao *et al.*[102] reported Mxenes-based catalysts for NRR electrocatalysis. The nitrogen fixation performance of the electrocatalyst is closely related to charge transfer. Since the charge transfer on Mo_2C and W_2C nanosheets is easier and their reaction energy is relatively low, they have high activity for N_2 fixation.

Huang *et al.*[91] applied DFT calculations to show that medium titanium on the edge plane is the most active site. The FE of MXene/FeOOH is higher than that of MXene/stainless-steel mesh, but its NH_3 yield is lower. The author attributed this phenomenon to the low conductivity and large charge transfer resistance of MXene/FeOOH. This information indicates that the optimal performance of N_2 reduction depends on the improvement of the electrocatalyst itself. Gao *et al.*[92] calculated that the overpotentials of Fe/$Ti_3C_2O_2$, Co/$Ti_3C_2O_2$, Ru/$Ti_3C_2O_2$ and Rh/$Ti_3C_2O_2$ for different TM single-atom supported $Ti_3C_2O_2$ catalysts using DFT are 0.92, 0.89, 1.16 and 0.84 eV, rescpectively. The terminal N_2 exhibits different potentials required for NH_3 synthesis, ranging from 0.68 eV to 2.33 eV. These catalysts can change the reaction path and avoid the traditional N≡N bond breaking obstacles. Similarly, Huang *et al.*[93] reported that Mo_2CO_2 or Ti_2CO_2 anchored by a single Ru or Mo atom has high electrocatalytic NRR activity, and at a potential of –0.64 V, N_2 can be effectively reduced to NH_3 on Ti@Mo_2CO_2 through different paths, as shown in Fig.9(A)—(D). In addition, by comparing the Gibbs free energy of each N_2 and H_2 and the protonation and hydrogen adsorption of the first N_2, the activity and selectivity of electro-catalytic NRR for Mo@Mo_2CO_2 was evaluated. It was found that the reduction of N_2 was performed through a remote or mixed mechanism, as shown in Fig.9(E)—(G). The results indicate that Mo@Mo_2CO_2 is a powerful electrocatalyst for electrocatalytic NRR. Gao *et al.*[94] designed a Mo_2TiC_2 high-efficiency NRR electrocatalyst. By comparing the overpotential(–0.74 V) with HER, the Mo_2TiC_2 MXenes electrocatalyzes the conversion of N_2 to NH_3 through the dissociation mechanism and the overpotential is –0.26 V. This process suppresses the evolution of H_2 and has a high electrocatalytic activity.

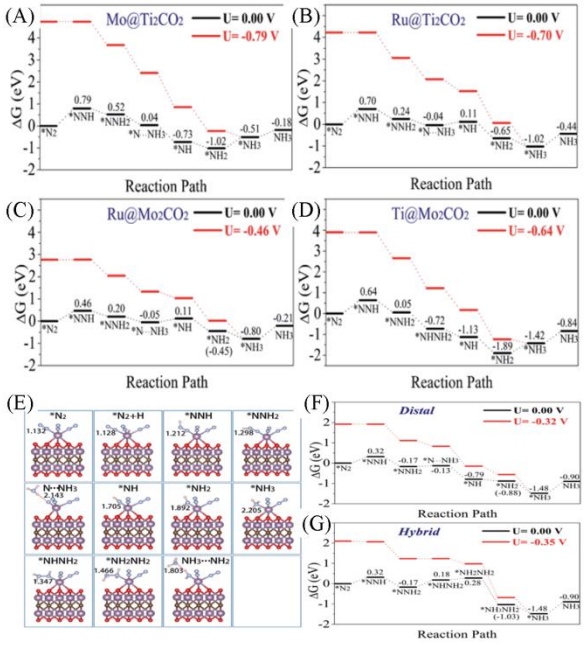

Fig.9 Free energy diagrams toward the production of NH_3 on catalysts and ways of catalyst reaction[93]

(A) $Mo@Ti_2CO_2$; (B) $Ru@Ti_2CO_2$; (C) $Ru@Mo_2CO_2$; (D) $Ti@Mo_2CO_2$ at zero and applied potentials(limiting potential); (E) optimized structures of possible intermediates *via* distal and hybrid mechanisms with two pre-adsorbed spectator dinitrogen molecules on $Mo@Mo_2CO_2$. Free energy diagrams of distal(F) and hybrid(G) mechanisms for $Mo@Mo_2CO_2$ at zero and applied limiting potentials, Copyright 2019, Royal Society Chemistry.

4.3.2 Experimental Progress

Wang's group[68] conducted DFT calculations and proved the existence of adsorption active sites in MXene. The Ti atoms have the maximum adsorption energy for binding N_2. Based on this, the electrocatalyst $Ti_3C_2T_x$ MXene synthesized in FeOOH nanosheets had a high FE value(5.78%). The experimental results show that it is important to maximize the exposure of edge sites in 2D-MXene electrocatalyst ammonia synthesis and to select metal hosts with low HER activity. Similarly, Sun's group[69] reported that $Ti_3C_2T_x$(T=F, OH) nanosheets with excellent selectivity and structural stability act as high-performance 2D NRR electrocatalysts for the conversion of environmental N_2 to NH_3. In 0.1 mol/L HCl, such catalysts can achieve a large NH_3 yield of 20.4 $\mu g \cdot h^{-1} \cdot mg^{-1}$cat and a high FE of 9.3% at –0.4 V(*vs*. RHE). DFT calculations show that the final reaction product of $^*NH_2$ is NH_3, which is the rate-limiting step. Zhang's group[70] reported that small-size, F-free $Ti_3C_2T_x$(T=O, OH) nanosheets as NRR catalysts have size effects and F-free properties. These features make the efficiency approximately twice that of F-based processing. In 0.1 mol/L HCl, the prepared material has a high NH_3 yield(36.9 $\mu g \cdot h^{-1} \cdot mg^{-1}$cat) and an FE(9.1%) at –0.3 V(*vs*. RHE).

Liu *et al.*[71] reported a high-performance $Ru@Ti_3C_2$ MXene catalyst for environmental electrocatalytic NRR. In 0.1 mol/L KOH electrolyte, the NH_3 yield of the Ru@MXene catalyst reached 2.3 $\mu mol \cdot h^{-1} \cdot cm^{-2}$. In addition, the FE was 13.13% at –0.4 V(*vs*. RHE). Li *et al.*[72] for the first time combined TiO_2 and $Ti_3C_2T_x$ to lead to a Ti-based NRR electrocatalyst with synergistic activity. When tested in 0.1 mol/L HCl, it can provide an NH_3 yield of 26.32 $\mu g \cdot h^{-1} \cdot mg^{-1}$ cat, and it has an FE of 8.42% at –0.60 V(*vs*. RHE), which is greater than those of TiO_2 and $Ti_3C_2T_x$. Fang *et al.*[73] reported *in-situ* growth of TiO_2 nanoparticles on $Ti_3C_2T_x$ nanosheets($TiO_2/Ti_3C_2T_x$), and their morphological structure is shown in Fig.10. $Ti_3C_2T_x$ plays an important role in the catalyst, which not only has high conductivity but also prevents the aggregation of TiO_2 nanoparticles. At the same time, TiO_2 nanoparticles rich in O vacancies enhance the surface specific area of $Ti_3C_2T_x$ nanosheets. The electrocatalyst showed an NH_3 yield of 32.17 $\mu g \cdot h^{-1} \cdot mg^{-1}$ cat at –0.55 V. In 0.1 mol/L HCl, the FE was 16.07% relative to RHE at –0.45 V. Finally, the author proves through theoretical simulation that $TiO_2(101)/Ti_3C_2T_x$ has the lowest NRR energy barrier(0.40 eV) compared to $Ti_3C_2T_x$ or $TiO_2(101)$ alone. The author[74] also proposed $Ti_3C_2T_x$ modified with MnO_2(T=F, OH) MXene nanohybrid(MnO_2-$Ti_3C_2T_x$) has good selectivity and stability. At –0.55 V(*vs*. RHE), 0.1 mol/L HCl can achieve a large NH_3 yield of 34.12 $\mu g \cdot h^{-1} \cdot mg^{-1}$cat and a high FE of 11.39%.

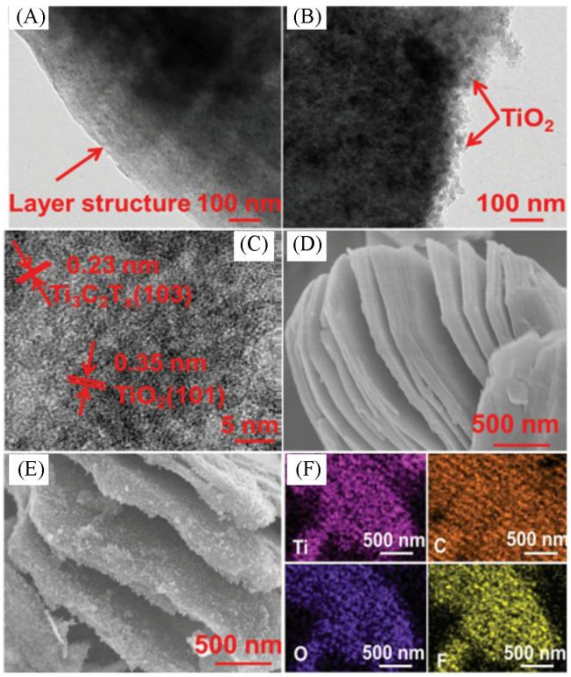

Fig.10 Characterization of the $TiO_2/Ti_3C_2T_x$[73]

(A) and (D) TEM and SEM images of the $Ti_3C_2T_x$; (B), (C) and (E) TEM, HRTEM and SEM images of the $TiO_2/Ti_3C_2T_x$; (F) elemental mapping images of C, Ti, O, and F in $TiO_2/Ti_3C_2T_x$, Copyright 2019, Wiley-VCH.

4.4 Other Layered 2D TM Materials

2D TM nanomaterials are good candidates for the construction of highly efficient and stable NRR electrocatalysts. The preparation of novel 2D TM electrocatalytic materials by similar doping composites has been extensively studied. At the same time, the recombination between 2D TM materials will also be a good NRR electrocatalyst. These strategies have opened up a new way to design new 2D TM materials and electrocatalysts. The 2D pentagonal TM phosphide(penta-MP, M=Ti, Zr, Hf) reported by Huang's group[103] is an effective NRR electrocatalyst. Through DFT calculation and *ab initio* molecular dynamics simulation, the author can predict that

penta-MP has dynamic, thermal and mechanical stability. Their quasi-planar structure and metal properties promote the strong adsorption of N_2 on the surface.

5 Conclusions and Outlook

This review summarizes the latest research on electrocatalysts based on 2D TM compounds and their composite materials in NRR. The development of high-efficiency NRR electrocatalysts based on 2D TM nanomaterials is summarized in terms of theoretical simulation and experimental progress. So far, great progress has been made in the development of electrocatalysts for NRR. Based on this, the conclusion of these works is based on the following points to achieve efficient electrocatalytic NRR ammonia synthesis.

2D TM nanomaterials utilize their own electronic structural characteristics and the vacancies. They can be hybrid with other nanoparticles to improve the dispersibility, forming electrocatalytic NRR candidate materials with high stability, high efficiency and durability. Between the noble metal and the 2D TM, the electronic structure can be adjusted by adjusting the size of the nanoparticles, thereby achieving more efficient NRR performance. The high efficiency can also be achieved through the synergistic effect with the vacancy. Non-precious metals can participate in the adjustment and change the 2D TM electronic structure and vacancies, forming O and S vacancies to lower the energy barrier and activate nitrogen molecules. The designed interface accelerates the reaction kinetics through the heterojunction formed between the layers, which can improve the conductivity and structural integrity of the heterojunction, and realize high efficiency. Doping with other elements can induce enhanced surface conductivity and d-band center, and significantly improve the selectivity of NH_3 electrosynthesis by adjusting the active site and preventing hydrogen release activity.

2D TM compounds have played a great role as NRR catalysts for the construction of high-efficiency electrocatalysis. However, compared to industrial ammonia synthesis technology, electrocatalytic ammonia synthesis still has a long way to go. Most of the electrocatalyst synthesis ammonia based on 2D TM compounds has a much lower yield than industrial synthesis ammonia. Currently, only a few electrocatalysts based on 2D TM compounds have relatively high stability to NRR. There is still much room for development to achieve industrial development. Therefore, it is still very attractive to explore the use of 2D TM compound catalysts to conduct the electrocatalytic synthesis of ammonia under ambient conditions. In addition, for most electrocatalysts based on 2D TM compounds, there are many controversies in the NRR process. The true active site is usually different from the active site on the original catalyst. In order to increase the electrocatalytic activity, we must fully understand the comprehensive understanding of the catalytic mechanism and electronic behavior. Recently, *in-situ* characterization has been developed. But it is not enough to fully understand the actual catalytic reaction activity. To clarify the actual catalytic reaction process, it is bound to develop more practical and reliable *in situ* analysis techniques. Therefore, the structure-activity relationship of electrocatalytic NRR can be obtained by observing the change of catalyst structure and information conversion, so as to guide the development of efficient NRR electrocatalyst with a better theoretical basis.

Acknowledgments

We gratefully appreciated MOE under AcRF Tier 1 RG4/17, AcRF Tier 2 MOE2016-T2-1-131.

References

[1] Crabtree G. W., Dresselhaus M. S., Buchanan M. V., *Phys Today*, **2004**, *57*, 39
[2] Nocera D. G., *Acc. Chem. Res.*, **2012**, *45*, 767
[3] Zhu X., Mou S., Peng Q., Liu Q., Luo Y., Chen G., Gao S., Sun X., *J. Mater. Chem. A*, **2020**, *8*, 1545
[4] Yin H., Dou Y., Chen S., Zhu Z., Liu P., Zhao H., *Adv. Mater.*, **2020**, *32*, 1904870
[5] Gilbert N., *Nature*, **2012**, *483*, 525
[6] Schlogl R., *Angew. Chem. Int. Ed. Engl.*, **2003**, *42*, 2004
[7] Klerke A., Christensen C. H., Norskov J. K., Vegge T., *J. Mater. Chem.*, **2008**, *18*, 2304
[8] Kuang M., Wang Y., Fang W., Tan H., Chen M., Yao J., Liu C., Xu J., Zhou K., Yan Q., *Adv. Mater.*, **2020**, 2002189
[9] Chen C., Zhu X., Wen X., Zhou Y., Zhou L., Li H., Tao L., Li Q., Du S., Liu T., Yan D., Xie C., Zou Y., Wang Y., Chen R., Huo J., Li Y., Cheng J., Su H., Zhao X., Cheng W., Liu Q., Lin H., Luo J., Chen J., Dong M., Cheng K., Li C., Wang S., *Nat. Chem.*, **2020**, 1, 1755
[10] Guo C. X., Ran J. R., Vasileff A., Qiao S. Z., *Energ. Environ. Sci.*, **2018**, *11*, 45
[11] van Der Ham C. J., Koper M. T., Hetterscheid D. G., *Chem. Soc. Rev.*, **2014**, *43*, 5183
[12] Tanabe Y., Nishibayashi Y., *Coordin. Chem. Rev.*, **2013**, *257*, 2551
[13] Rod T. H., Logadottir A., Norskov J. K., *J. Chem. Phys.*, **2000**, *112*, 5343
[14] Jia H. P., Quadrelli E. A., *Chem. Soc. Rev.*, **2014**, *43*, 547
[15] Tan C., Cao X., Wu X. J., He Q., Yang J., Zhang X., Chen J., Zhao W., Han S., Nam G. H., Sindoro M., Zhang H., *Chem. Rev.*, **2017**, *117*, 6225
[16] Dong R., Zhang T., Feng X., *Chem. Rev.*, **2018**, *118*, 6189
[17] Novoselov K. S., Geim A. K., Morozov S. V., Jiang D., Zhang Y., Dubonos S. V., Grigorieva I. V., Firsov A. A., *Science*, **2004**, *306*, 666
[18] Jin H., Guo C., Liu X., Liu J., Vasileff A., Jiao Y., Zheng Y., Qiao S. Z., *Chem. Rev.*, **2018**, *118*, 6337
[19] Yang Q., Su Y., Chi C., Cherian C. T., Huang K., Kravets V. G., Wang F. C., Zhang J. C., Pratt A., Grigorenko A. N., Guinea F., Geim A. K., Nair R. R., *Nat. Mater.*, **2017**, *16*, 1198
[20] Peng J., Dong W., Wang Z., Meng Y., Liu W., Song P., Liu Z., *Materials Today Advances*, **2020**, *8*, 10081
[21] Chia X. Y., Pumera M., *Nat. Catal.*, **2018**, *1*, 909
[22] Cui X. Y., Tang C., Zhang Q., *Adv. Energy Mater.*, **2018**, *8*, 1800369
[23] Lu Q., Yu Y., Ma Q., Chen B., Zhang H., *Adv. Mater.*, **2016**, *28*, 1917
[24] Yu L. L., Qin J. Z., Zhao W. J., Zhang Z. G., Ke J., Liu B. J., *Int. J. Photoenergy*, **2020**, *2020*, 5251431
[25] Li Q. Y., He L. Z., Sun C. H., Zhang X. W., *J Phys. Chem. C*, **2017**,

121, 27563

[26] Abghoui Y., Garden A. L., Hlynsson V. F., Bjorgvinsdottir S., Olafsdottir H., Skulason E., *Phys. Chem. Chem. Phys.*, **2015**, *17*, 4909

[27] Hu B., Hu M., Seefeldt L., Liu T. L., *ACS. Energy Lett.*, **2019**, *4*, 1053

[28] Lv C., Qian Y., Yan C., Ding Y., Liu Y., Chen G., Yu G., *Angew. Chem. Int. Ed. Engl.*, **2018**, *57*, 10246

[29] Shipman M. A., Symes M. D., *Catal Today*, **2017**, *286*, 57

[30] Ling C., Zhang Y., Li Q., Bai X., Shi L., Wang J., *J. Am. Chem. Soc.*, **2019**, *141*, 18264

[31] Laird T. J. O. P. R., *Development*, **1997**, *1*, 391

[32] Fang Y., Xue Y., Li Y., Yu H., Hui L., Liu Y., Xing C., Zhang C., Zhang D., Wang Z., Chen X., Gao Y., Huang B., Li Y., *Angew. Chem. Int. Ed. Engl.*, **2020**, *59*, 2

[33] Bao D., Zhang Q., Meng F. L., Zhong H. X., Shi M. M., Zhang Y., Yan J. M., Jiang Q., Zhang X. B., *Adv. Mater.*, **2017**, *29*, 1604799

[34] Vanselow A. P. J. I., Edition E. C. A., **1939**, *12*, 516

[35] Yang D. S., Chen T., Wang Z. J., *J. Mater. Chem. A*, **2017**, *5*, 18967

[36] Bao D., Zhang Q., Meng F. L., Zhong H. X., Shi M. M., Zhang Y., Yan J. M., Jiang Q., Zhang X. B., *Adv. Mater.*, **2017**, *29*, 1604799.1

[37] Licht S., Cui B., Wang B., Li F. F., Lau J., Liu S., *Science*, **2014**, *345*, 637

[38] Thomas D. H., Rey M., Jackson P. E., *J. Chromatogr. A*, **2002**, *956*, 181

[39] Michalski R., Kurzyca I., *Polish Journal of Environmental Studies*, **2006**, *15*, 5

[40] Michalski R., *Crit. Rev. Anal. Chem.*, **2009**, *39*, 230

[41] Bruzzoniti M. C., de Carlo R. M., Fungi M., *J. Sep. Sci.*, **2008**, *31*, 3182

[42] Zhu Y., Yuan D. X., Huang Y. M., Ma J., Feng S. C., Lin K. N., *Marine Chemistry*, **2014**, *162*, 114

[43] Zhang L., Ji X., Ren X., Ma Y., Shi X., Tian Z., Asiri A. M., Chen L., Tang B., Sun X., *Adv. Mater.*, **2018**, *30*, 1800191

[44] Zhou Y., Yu X. P., Wang X. Y., Chen C., Wang S. T., Zhang J., *Electrochim Acta*, **2019**, *317*, 34

[45] Suryanto B. H. R., Wang D., Azofra L. M., Harb M., Cavallo L., Jalili R., Mitchell D. R. G., Chatti M., MacFarlane D. R., *ACS Energy Lett.*, **2018**, *4*, 430

[46] Liang J., Ma S., Li J., Wang Y., Wu J., Zhang Q., Liu Z., Yang Z., Qu K., Cai W., *J. Mater. Chem. A*, **2020**, *8*, 10426

[47] Zhang J., Tian X., Liu M., Guo H., Zhou J., Fang Q., Liu Z., Wu Q., Lou J., *J. Am. Chem. Soc.*, **2019**, *141*, 19269

[48] Li X. H., Ren X., Liu X. J., Zhao J. X., Sun X., Zhang Y., Kuang X., Yan T., Wei Q., Wu D., *J. Mater. Chem. A*, **2019**, *7*, 2524

[49] Zhao X., Lan X., Yu D., Fu H., Liu Z., Mu T., *Chem. Commun.(Camb.)*, **2018**, *54*, 13010

[50] Wang H. B., Wang J. Q., Zhang R., Cheng C. Q., Qu K. W., Yang Y. J., Mao J., Liu H., Du M., Dong C. K., Du X. W., *ACS Catal.*, **2020**, *10*, 4914

[51] Li P., Fu W., Zhuang P., Cao Y., Tang C., Watson A. B., Dong P., Shen J., Ye M., *Small*, **2019**, *15*, 1902535

[52] Lai F. L., Chen N., Ye X. B., He G. J., Zong W., Holt K. B., Pan B. C., Parkin I. P., Liu T. X., Chen R. J., *Adv. Funct. Mater.*, **2020**, *30*, 1907376

[53] Jia K., Wang Y., Qiu L., Gao J. J., Pan Q., Kong W. H., Zhang X. X., Alshehri A. A., Alzahrani K. A., Zhong B. H., Guo X. D., Yang L., *Inorg. Chem. Front.*, **2019**, *6*, 1986

[54] Chu K., Wang J., Liu Y. P., Li Q. Q., Guo Y. L., *J. Mater. Chem. A*, **2020**, *8*, 7117

[55] Wang Y., Chen A. R., Lai S. H., Peng X. Y., Zhao S. Z., Hu G. Z., Qiu Y., Ren J. Q., Liu X. J., Luo J., *J. Catal.*, **2020**, *381*, 78

[56] Fang C. H., Bi T., Xu X. X., Yu N., Cui Z. Q., Jiang R. B., Geng B. Y., *Adv. Mater. Interfaces.*, **2019**, *6*, 1901034

[57] Zhang R., Ren X., Shi X., Xie F., Zheng B., Guo X., Sun X., *ACS Appl. Mater. Interfaces*, **2018**, *10*, 28251

[58] Li X. H., Li L., Ren X., Wu D., Zhang Y., Ma H. M., Sun X., Du B., Wei Q., Li B. H., *Ind. Eng. Che. Res.*, **2018**, *57*, 16622

[59] Han J. R., Ji X. Q., Ren X., Cui G. W., Li L., Xie F. Y., Wang H., Li B. H., Sun X. P., *J. Mater. Chem. A*, **2018**, *6*, 12974

[60] Kong W., Zhang R., Zhang X., Ji L., Yu G., Wang T., Luo Y., Shi X., Xu Y., Sun X., *Nanoscale*, **2019**, *11*, 19274

[61] Zhao S., Liu H. X., Qiu Y., Liu S. Q., Diao J. X., Chang C. R., Si R., Guo X. H., *J. Mater. Chem. A*, **2020**, *8*, 6586

[62] Cheng S., Gao Y. J., Yan Y. L., Gao X., Zhang S. H., Zhuang G. L., Deng S. W., Wei Z. Z., Zhong X., Wang J. G., *J. Energy Chem.*, **2019**, *39*, 144

[63] Zheng J., Lyu Y., Qiao M., Veder J. P., Marco R. D., Bradley J., Wang R., Li Y., Huang A., Jiang S. P., Wang S., *Angew. Chem. Int. Ed. Engl.*, **2019**, *58*, 18604

[64] Liu Y. T., Chen X., Yu J., Ding B., *Angew. Chem. Int. Ed. Engl.*, **2019**, *58*, 18903

[65] Chen Y. J., Wu B., Sun B. L., Wang N., Hu W. C., Komarneni S., *ACS Sustain. Chem. Eng.*, **2019**, *7*, 18874

[66] Wang X. H., Wang J., Li Y. B., Chu K., *Chemcatchem*, **2019**, *11*, 4529

[67] Liu Y. P., Li Y. B., Zhang H., Chu K., *Inorg. Chem.*, **2019**, *58*, 10424

[68] Luo Y. R., Chen G. F., Ding L., Chen X. Z., Ding L. X., Wang H. H., *Joule*, **2019**, *3*, 279

[69] Zhao J., Zhang L., Xie X. Y., Li X., Ma Y., Liu Q., Fang W. H., Shi X., Cui G., Sun X., *J. Mater. Chem. A*, **2018**, *6*, 24031

[70] Li T., Yan X., Huang L., Li J., Yao L., Zhu Q., Wang W., Abbas W., Naz R., Gu J., Liu Q., Zhang W., Zhang D., *J. Mater. Chem. A*, **2019**, *7*, 14462

[71] Liu A., Gao M., Ren X., Meng F., Yang Y., Yang Q., Guan W., Gao L., Liang X., Ma T., *Nanoscale*, **2020**, *12*, 10933

[72] Zhang J., Yang L., Wang H., Zhu G., Wen H., Feng H., Sun X., Guan X., Wen J., Yao Y., *Inorg. Chem.*, **2019**, *58*, 5414

[73] Fang Y. F., Liu Z. C., Han J. R., Jin Z. Y., Han Y. Q., Wang F. X., Niu Y. S., Wu Y. P., Xu Y. H., *Adv. Energy Mater.*, **2019**, *9*, 1803406

[74] Kong W., Gong F., Zhou Q., Yu G., Ji L., Sun X., Asiri A. M., Wang T., Luo Y., Xu Y., *J. Mater. Chem. A*, **2019**, *7*, 18823

[75] Zhang L., Ji X. Q., Ren X., Luo Y. L., Shi X. F., Asiri A. M., Zheng B. Z., Sun X. P., *ACS Sustain Chem. Eng.*, **2018**, *6*, 9550

[76] Zhang R., Zhang Y., Ren X., Cuo G. W., Asiri A. M., Zheng B. Z., Sun X. P., *ACS Sustain Chem. Eng.*, **2018**, *6*, 9545

[77] Jin H., Li L., Liu X., Tang C., Xu W., Chen S., Song L., Zheng Y., Qiao S. Z., *Adv. Mater.*, **2019**, *31*, 1902709

[78] Zhang R., Ji L., Kong W., Wang H., Zhao R., Chen H., Li T., Li B., Luo Y., Sun X., *Chem. Commun.(Camb.)*, **2019**, *55*, 5263

[79] Yu J., Li C., Li B., Zhu X., Zhang R., Ji L., Tang D., Asiri A. M., Sun X., Li Q., Liu S., Luo Y., *Chem. Commun.(Camb.)*, **2019**, *55*,

6401

[80] Wu D., Wang H., Huang H., Zhang R., Ji L., Chen H., Luo Y., You J., Tang D., Zhang Z., Sun X., *Chem. Commun.(Camb.)*, **2019**, *55*, 7546

[81] Wang H., Si J., Zhang T., Li Y., Yang B., Li Z., Chen J., Wen Z., Yuan C., Lei L., Hou Y., *Appl. Catal.*, *B*, **2020**, *270*, 118892

[82] Li F., Tang Q., *Nanoscale*, **2019**, *11*, 18769

[83] Ma B. Y., Peng Y., Ma D. W., Deng Z., Lu Z. S., *Appl. Surf. Sci.*, **2019**, *495*, 143463

[84] Li M., Cui Y., Sun L., Zhang X., Peng L., Huang Y., *Inorg. Chem.*, **2020**, *59*, 4858

[85] Zhai X., Li L., Liu X., Li Y., Yang J., Yang D., Zhang J., Yan H., Ge G., *Nanoscale*, **2020**, *12*, 10035

[86] Yang T., Song T. T., Zhou J., Wang S. J., Chi D. Z., Shen L., Yang M., Feng Y. P., *Nano Energy*, **2020**, *68*, 104304

[87] Guo H., Li L., Wang X., Yao G., Yu H., Tian Z., Li B., Chen L., *ACS Appl. Mater. Interfaces*, **2019**, *11*, 36506

[88] Yang L., Chen F., Song E., Yuan Z., Xiao B., *ChemPhysChem*, **2020**, *21*, 1235

[89] Li L., Li B. H., Guo Q. Y., Li B., *J. Phys. Chem. C*, **2019**, *123*, 14501

[90] Naguib M., Kurtoglu M., Presser V., Lu J., Niu J., Heon M., Hultman L., Gogotsi Y., Barsoum M. W. J. A. M., **2011**, *23*, 4248

[91] Huang L., Gu X., Zheng G., *Chem-US*, **2019**, *5*, 15

[92] Gao Y. J., Zhuo H., Cao Y. Y., Sun X., Zhuang G. L., Deng S. W., Zhong X., Wei Z. Z., Wang J. G., *Chinese J. Catal.*, **2019**, *40*, 152

[93] Huang B., Li N., Ong W. J., Zhou N. G., *J. Mater. Chem. A*, **2019**, *7*, 27620

[94] Gao Y. J., Cao Y. Y., Zhuo H., Sun X., Gu Y. B., Zhuang G. L., Deng S. W., Zhong X., Wei Z. Z., Li X. N., Wang J. G., *Catal. Today*, **2020**, *339*, 120

[95] Peng C., Yang X., Li Y., Yu H., Wang H., Peng F., *ACS Appl. Mater. Interfaces*, **2016**, *8*, 6051

[96] Azofra L. M., Li N., MacFarlane D. R., Sun C., *Energ. Environ. Sci.*, **2016**, *9*, 2545

[97] Abghoui Y., Garden A. L., Hlynsson V. F., Bjrgvinsdóttir S., Lafsdóttir H., Skúlason E. *Phys. Chem. Chem. Phys*, **2015**, *17,* 4909

[98] Abghoui Y., Skúlasson E., *Procedia Computer Science*, **2015**, *51*, 1897

[99] Abghoui Y., Garden A. L., Howalt J. G., Vegge T., Skúlason E., *ACS Catal.*, **2015**, *6*, 635

[100] Abghoui Y., Skulason E., *Catal. Today*, **2017**, *286*, 69

[101] Abghoui Y., Skulason E., *J. Phys. Chem. C*, **2017**, *121*, 6141

[102] Shao M., Shao Y., Chen W., Ao K. L., Tong R., Zhu Q., Chan I. N., Ip W. F., Shi X., Pan H., *Phys. Chem. Chem. Phys.*, **2018**, *20*, 14504

[103] Ying Y. R., Fan K., Luo X., Huang H. T., *J. Mater. Chem. A*, **2019**, *7*, 11444